Title

Cortical bone laminar analysis reveals increased midcortical and periosteal porosity in type 2 diabetic postmenopausal women with history of fragility fractures compared to fracture-free diabetics

Journal

Osteoporosis International, 27(9)

ISSN

0937-941X

Authors

Heilmeier, U

Cheng, K

Pasco, C

et al.

Publication Date

2016-09-01

DOI

10.1007/s00198-016-3614-7

Peer reviewed

HHS Public Access

Author manuscript

Osteoporos Int. Author manuscript; available in PMC 2019 August 08.

Published in final edited form as:

Osteoporos Int. 2016 September ; 27(9): 2791–2802. doi:10.1007/s00198-016-3614-7.

Cortical bone laminar analysis reveals increased midcortical and periosteal porosity in type 2 diabetic postmenopausal women with history of fragility fractures compared to fracture-free diabetics

U. Heilmeier[1], **K. Cheng**[2], **C. Pasco**[2], **R. Parrish**[2], **J. Nirody**[3], **J. M. Patsch**[1,4], **C. A. Zhang**[5], **G. B. Joseph**[1], **A. J. Burghardt**[1], **A. V. Schwartz**[5], **T. M. Link**[1], **G. Kazakia**[1]

[1]Musculoskeletal Quantitative Imaging Research Group, Department of Radiology & Biomedical Imaging, University of California San Francisco, 185 Berry Street, San Francisco, CA 94158, USA

[2]Department of Bioengineering, University of California Berkeley, 306 Stanley Hall, Berkeley, CA 94720, USA

[3]Biophysics Graduate Group, University of California Berkeley, 574 Stanley Hall, MC 3220, Berkeley, CA 94720, USA

[4]Department of Biomedical Imaging and Image-Guided Therapy, Medical University of Vienna, Waehringer Guertel 18-20, 1090 Vienna, Austria

[5]Department of Epidemiology and Biostatistics, University of California San Francisco, 550 16th Street, San Francisco, CA 94158, USA

Abstract

Summary—We investigated the characteristics and spatial distribution of cortical bone pores in postmenopausal women with type 2 diabetes (T2D). High porosity in the midcortical and periosteal layers in T2D subjects with fragility fractures suggests that these cortical zones might be particularly susceptible to T2D-induced toxicity and may reflect cortical microangiopathy.

Introduction—Elevated cortical porosity is regarded as one of the main contributors to the high skeletal fragility in T2D. However, to date, it remains unclear if diabetic cortical porosity results from vascular cortical changes or from an expansion in bone marrow space. Here, we used a novel cortical laminar analysis technique to investigate the characteristics and spatial radial distribution of cortical pores in a T2D group with prior history of fragility fractures (DMFx, assigned high-risk group) and a fracture-free T2D group (DM, assigned low-risk group) and to compare their results to non-diabetic controls with (Fx) and without fragility fractures (Co).

Methods—Eighty postmenopausal women (n = 20/group) underwent high-resolution peripheral quantitative computed tomography (HR-pQCT) of the distal tibia and radius. Cortical bone was divided into three layers of equal width including an endosteal, midcortical, and periosteal layer. Within each layer, total pore area (TPA), total pore number (TPN), and average pore area (APA)

U. Heilmeier Ursula.Heilmeier@ucsf.edu.

were calculated. Statistical analysis employed Mann-Whitney tests and ANOVA with post hoc tests.

Results—Compared to the DM group, DMFx subjects exhibited +90 to +365 % elevated global porosity (p=0.001). Cortical laminar analysis revealed that this increased porosity was for both skeletal sites confined to the midcortical layer, followed by the periosteal layer (midcortical +1327 % TPA, p≤0.001, periosteal +634 % TPA, p=0.002), and was associated in both layers and skeletal sites with high TPN (+430 % TPN, p<0.001) and high APA (+71.5 % APA, p<0.001).

Conclusion—High porosity in the midcortical and periosteal layers in the high-risk T2D group suggests that these cortical zones might be particularly susceptible to T2D-induced toxicity and may reflect cortical microangiopathy.

Keywords

Cortical bone laminar analysis; Cortical pore distribution; Cortical pore number; Cortical porosity; Diabetic bone disease; Type 2 diabetes

Introduction

Cortical bone is a major component of bone tissue that accounts for up to 80 % of the human skeleton's weight. Several studies have demonstrated that bone's mechanical competence and fracture resistance depend on cortical bone microstructural properties such as cortical porosity, crystallinity, and presence/absence of microcracks [1, 2]. In particular, cortical bone porosity has been found to contribute substantially to bone strength, stiffness, and fracture toughness [3–5]. In human cadaveric studies, differences in cortical porosity accounted for about 75 % of the observed age-related reduction in bone strength [6]. Similarly, cortical porosity explained up to 40 % of the variance in fracture toughness in human tibial bone most likely by reducing bone net loading area and therefore reducing the area for microcrack propagation [7].

Due to its relevance for bone fragility, cortical porosity has recently been studied as a potential predictor of fracture. In vivo studies have measured cortical porosity via high-resolution peripheral quantitative computed tomography (HR-pQCT) and focused on those diseased populations, in which conventional methods of fracture risk assessment such as dual X-ray absorptiometry (DXA) or the WHO-fracture risk assessment tool (FRAX) may underestimate the true fracture risk. Their findings demonstrated that cortical porosity of the compact-appearing cortex predicted prevalent forearm fractures in osteopenic postmenopausal women independent of areal bone mineral density (aBMD) and WHO-FRAX score [8]. In addition, recent intervention studies reported that pathological cortical porosity and its associated strength deficits are per se reversible by pharmacological treatment [9, 10]. These results indicate that cortical porosity may be an important target for treatment of bone fragility [11] and a promising radiologic endpoint for randomized controlled trials.

To date, in vivo HR-pQCT studies have not investigated the spatial distribution of cortical porosity within the cortex although cortical pores have been shown to be heterogeneously distributed throughout the cortex in early micrometer and videodensitometry studies [12,

13]. This is somewhat surprising as spatial pore distribution is an important co-determinant of bone strength [14], and understanding cortical porosity distribution can help generate hypotheses about the biological mechanisms that drive cortical porosity. Potential mechanisms include pore space enlargement by expansion of the marrow cavity, expansion of the vascular network in the cortex, or both. Within the compact cortex, formation of large cortical pores has been attributed to clustering of osteons and merging of Haversian canals [15]. At the endocortical border, “trabecularization” or marrow space expansion is hypothesized to drive observed increases in cortical porosity [16]. Multiple mechanisms of pore space expansion likely are at play in diabetic bone disease, and spatial distribution of porosity can shed light on which if these mechanisms is driving pathologic cortical porosity.

Spatial distribution assessment via in vivo methods such as HR-pQCT has been hampered by the lack of appropriate automated software tools. With the development of the HR-pQCT-based cortical laminar analysis technique [17], it is now possible to assess the spatial distribution of cortical pores on the order of 100 μm in diameter or larger within three concentric layers of the cortex. Here, we applied this novel technique to the cortical bone of type 2 diabetic (T2D) patients with history of fragility fractures who have been found to show increased amounts of cortical porosity [18, 19]. Our long-term goal is to better understand biological drivers and mechanical influences of cortical porosity in T2D. The primary goal of this study was to assess the nature and spatial distribution of cortical porosity by determining cortical pore number, size, and radial distribution within endosteal, midcortical, and periosteal layers of cortical bone in T2D postmenopausal women with history of fragility fractures (DMFx, high-risk fracture group [20]) and to compare them with T2D postmenopausal women without fractures (DM, low-risk fracture group). Our secondary goal was to assess these metrics in non-diabetic postmenopausal women with (Fx) and without history of fragility fractures (Co) and to compare our results to previously characterized cohorts.

Material and methods

Subjects

Eighty postmenopausal women were enrolled in this cross-sectional study as described in detail previously [18]. The study was HIPAA compliant, approved by the UCSF Committee on Human Research, and written informed content was given by all study participants prior to enrolment. Subjects were recruited into one of the following four study groups: (1) healthy controls, i.e., non-diabetic subjects without any history of fragility fracture (Co, n=20); (2) healthy, nondiabetic controls with a prior history of fragility fractures (Fx, n=20); (3) fracture-free T2D women (DM, n=20, assigned low-fracture risk group); and (4) T2D women with a positive history of fragility fractures after the onset of diabetes (DMFx, n=20, assigned high-fracture risk group).

Inclusion and exclusion criteria for this study have been listed in detail previously [18, 20]. To summarize, we only included postmenopausal women (aged 50–75 years, BMI between 18 and 37 kg/m^2) that were mobile and did not report any medical condition or medication use with known impact on bone metabolism [20]. Disqualifying medications included, e.g., the chronic (>6 months) intake of estrogens, adrenal or anabolic steroids, antacids,

anticoagulants, anticonvulsants, pharmacological doses of vitamin A, fluorides, bisphosphonates, calcitonin, tamoxifen, parathyroid hormone (PTH), or thiazolidinediones. For diabetics, diagnosis of T2D underlied the American Diabetes Association criteria [21]. In addition, T2D individuals had to be on antidiabetic treatment by oral therapies and/or insulin for a minimum of 3 years. Subjects with fragility fractures were only enrolled if their fracture met the criteria for a fragility fracture defined as low-energy fracture sustained during a fall from standing height or less. Moreover, fractures had to be remote (as verified by history, radiographs, and by spinal MRI screening for acute occult fractures) [20]. Subjects presenting with fractures of other origin (such as pathologic fractures through tumors, tumor-like lesions, or sustained from a high-energy trauma) were excluded from the study.

Laboratory analyses

Blood samples were obtained between 8 and 11 a.m. from all subjects after an overnight fast. Blood was allowed to clot in an upright position for 40 min and then centrifuged at 2500 rpm for 15 min within 1 h of collection. Serum was subsequently transferred to 1.5-mL plastic screw cap vials and immediately sent for basic blood workup. Remaining serum aliquots were rapidly frozen and stored at −70 °C until further analysis. At Quest Diagnostics, concentrations of blood glucose (mg/dL), HbA1c (%), parathyroid hormone (PTH) (pg/mL), total 25-hydroxyvitamin D (ng/mL), and serum creatinine (mg/dL) were determined. To estimate glomerular filtration rate (eGRF), the Modification of Diet in Renal Disease equation (MDRD) was applied and glomerular filtration rates were corrected accordingly for race in African- American women [22, 23].

HR-pQCT imaging

The distal tibia and distal radius of all patients were scanned using the same clinical HR-pQCT system manufactured by Scanco Medical AG (XtremeCT, Scanco Medical AG, Brüttisellen, Switzerland). Although the ultradistal scan sites have been established as the standard HR-pQCT acquisition sites for trabecular analysis [24, 25], the distal scan sites cover a portion of the diaphysis with a relatively higher ratio of cortical bone to trabecular bone. As the goal of this present study was to analyze the laminar pore distribution within the cortex, we therefore focused HR-pQCT imaging on these distal scan sites. A well-established in vivo standard imaging protocol with 60 kVP, 900 mA, 100-ms integration time, and 126-mm field of view as imaging parameters was used [26, 27]. In general, the tibia and the radius of the non-dominant body side were scanned. In case the patient reported a history of fracture at the non-dominant upper or lower extremity, the contralateral tibia or radius was imaged, respectively. For the scans, the patient’s extremity was immobilized in a carbon fiber cast and anchored in the scanner to minimize motion. A single anteroposterior scout radiograph was obtained to allow correct positioning of the tomographic scan volume. A reference line was first placed along the tibial and radial midjoint, and a scan region was identified from the scout view using a fixed offset of 37.5 mm proximal to the reference line at the tibia and a fixed offset of 24.5 mm for the radius [18]. For each skeletal site, a total scan volume encompassing 9.02 mm in length (110 slices) proximal from the offset was then acquired. Per scan, 750 projections were obtained and the effective patient dose was estimated at 3 μSv. Average time per scan was 2.8 min. Images were reconstructed to a

1536×1536 matrix, allowing for a final nominal resolution of 82 μm isotropic voxels. To calculate densitometric bone parameters, image attenuation values were calibrated against the attenuation values derived from a standardized hydroxyapatite (HA) phantom that was imaged daily on the scanner for quality assurance. To account for potential image motion, all acquired scans were visually scored for presence and severity of motion artifacts using the manufacturer's artifact grading scheme [28]. Only scans with image quality scores of 1 to 3 were utilized for further image analysis. In total, 79 out of 80 tibia scans and 74 of 80 radius scans fulfilled the image quality criteria and were available for image analysis.

Image analysis

Cortical segmentation—For both skeletal sites, initial contours of the cortical bone compartment were created using a semi-automated three-step imaging processing chain, as described in detail previously by Burghardt et al. [29]. In a first step, a chaperoned iterative autocontouring process was employed to identify the periosteal and endosteal cortical margins from adjacent soft tissue and cancellous bone, respectively. The autocontours were then visually checked for accuracy by an experienced radiologist (JMP), and minor local corrections were made, if necessary. In a second step, the resolved pores within the cortical bone compartment were extracted (intracortical porosity segmentation) by using a combination of 2D connectivity filter and hysteresis region growing algorithm [29]. This method excludes transcortical foramina or surface erosions, as well as artifactual void due to endosteal or periosteal surface roughness. In the last step, the segmented cortical compartment and the intracortical porosity segmentation mask were digitally merged to create a final, refined mask of the cortical compartment. A customized image processing language (IPL v.506a-ucsf, Scanco Medical AG) with in-house functionality was used to carry out cortical segmentation.

Cortical bone laminar analysis—After cortical segmentation, the refined cortex was subdivided into three concentric regions of equal width corresponding to the endosteal, midcortical, and periosteal laminar layers as described in detail elsewhere [17, 30]. To attain this division, the inner and outer borders of the cortical compartment were first discretized. Next, midcortical boundaries were generated at points one-third and two-thirds between the endosteal and periosteal boundaries. Continuous boundaries were formed by a series of dilations followed by a thinning routine. To determine the location of pore skeletons for assignment to layers, a skeletonization procedure was utilized to deconstruct the pore network into individual elements [31]. Based on the location of its pore skeleton, each entire pore was then assigned to a laminar layer on a slice-by-slice basis. We refer the reader to Nirody et al. for further details on the division of the cortex and the assignment of pores to laminar layers [17]. Laminar analysis was performed using MATLAB (R2012a Student Version, The MathWorks, Inc.).

Quantification of cortical bone laminar analysis metrics—For each skeletal site, three layer-by-layer metrics were computed to characterize cortical porosity in more detail: total pore area (TPA, mm^2/mm^2), total pore number (TPN, mm^{-2}), and average pore area (APA, mm^2). In each slice of the analyzed volume, TPA was calculated as the sum of all pore areas assigned to a specific layer. TPN was calculated as the total number of pores

within each layer. Both TPA and TPN values were normalized by the area of each layer to account for different layer areas. APA was calculated as the mean pore area within each layer. All metrics are reported as means across all slices in the analyzed volume. Interscan reproducibilities of laminar cortical analysis metrics were assessed from two repeat acquisitions in 15 female subjects as described previously [17]. The computed root-mean-square coefficients (RMS-CV) ranged from 3.04 to 3.94 % for the midcortical TPN, TPA, and APA metrics, from 4.37 to 6.09 % for the periosteal metrics, and from 5.77 to 9.35 % for the endosteal TPN, TPA, and APA parameters [17].

Statistical analysis

The distribution of each variable was explored via visualization of histograms and Shapiro-Wilk tests. Intergroup differences in demographic and metabolic variables and differences in laminar metrics within each group were assessed using oneway analysis of variance (ANOVA) with subsequent post hoc Tukey-Kramer tests, independent *t*-tests, or Pearson's chisquared test as appropriate. For our primary comparison, we investigated laminar analysis metrics in the DMFx and DM groups via Mann-Whitney *U* tests or independent *t*-tests, respectively. For our secondary goals, laminar metrics were compared between Co and Fx subjects and Co and DM subjects using one-way ANOVAwith subsequent Tukey post hoc tests. To account for the slight difference in racial distribution between Co, DM, and Fx groups, we adjusted the ANOVA in these comparisons for race. Additional adjustment for age was employed in the Co-Fx comparison, as Fx patients were significantly older than controls. All analyses were performed using IBM SPSS® Statistics 20.0 (IBM, Armonk, NY) and STATA 11 software (StataCorp LP, College Station, TX, USA). Statistical significance was defined as $p<0.05$.

Results

Subject characteristics

As evident from Table 1, DMFx and DM groups exhibited similar demographic and anthropometric characteristics (age $p=0.117$, BMI $p=0.838$, and racial composition $p=0.667$). Both diabetic groups (DMFx and DM) showed similar levels of moderate to poorglycemic control (HbA1c>7 % $p=0.999$, fasting blood glucose levels>126 ng/mL $p=0.809$) and comparable levels of kidney function (eGFR $p=0.465$) and of bone regulating hormones such as PTH ($p=0.962$) or total 25-hydroxyvitamin D ($p=0.375$). The main difference between DMFx and DM subjects consisted in their diabetes duration with the DMFx group suffering for a significantly longer period of T2D compared to the DM group (DM 7.6 ±3.1 years; DMFx 13.3±8.8 years, $p=0.012$) [18]. With respect to the non-diabetic groups, control subjects (Co) were significantly younger than Fx patients ($p=0.001$) and exhibited lower total serum 25-hydroxyvitamin D levels than Fx subjects ($p=0.003$) but also showed less supplementary vitamin D intake upon chart review [18]. All other baseline characteristics were comparable among these two non-diabetic groups. Across both fracture groups (DMFx and Fx), we observed similar rates, sites, and ages of fragility fractures: overall, 55 skeletal fragility fractures were sustained in both groups. In both groups, fractures of any skeletal site were included. A detailed breakdown of the skeletal sites can be found elsewhere [18]. On average, subjects of the DMFx group had suffered their latest

fragility fracture 3.1±2.7 years ago, while participants of the Fx group had a mean fracture-free interval prior to study enrolment of about 3.3 ± 3.6 years (independent *t*-tests; $p = 0.837$). In each group, the fragility fractures were remote (>11 months old, Fx $n = 16$, DMFx $n = 17$), and none of the fragility fractures was sustained less than 5 months prior to the examination date. On spinal MRI screening, no occult acute vertebral fracture was detected in any of the four study groups [20].

Overall porosity parameters

When looking at the overall amount of porosity (global cortical porosity) in the distal tibia and radius cortex, we observed as in our original study [18] that DMFx subjects had significantly elevated global cortical porosity (tibia + 87.9 %, $p=0.011$; radius + 365.1 %, $p<0.0001$), larger pore volume (tibia + 95.3 %, $p=0.020$; radius +370.4 %, $p<0.0001$), and a higher variability in pore size (tibia + 19.3 %, $p=0.019$; radius +36.0 %, $p=0.035$) compared to fracture-free diabetics (DM) [18]. Diabetic subjects without fractures (DM) showed the lowest means in global cortical porosity of all four groups, but differences compared to control subjects were not significant ($p = 0.210$) nor were comparisons between unfractured (Co) and fractured non-diabetic controls (Fx) ($p=0.310$) [18].

Spatial pore distribution between groups

Results regarding the spatial cortical pore distribution are summarized in Tables 2 and 3 and are visually depicted for the DMFx and DM groups in Fig. 2.

When evaluating the radial distribution of pores within the tibial cortex, we observed that DMFx subjects demonstrated the greatest relative differences in midcortical and periosteal TPA, TPN, and APA compared to DM subjects. DMFx subjects exhibited up to 3-fold higher porosity in the midcortical layer (+271 % TPA in DMFx vs DM, $p=0.001$) and up to 2-fold higher porosity in the periosteal layer compared to DM subjects (+123 % TPA in DMFx vs DM, $p=0.028$). The endosteal layer showed comparable levels of TPA among both groups. High midcortical and periosteal porosity in DMFx patients was associated with higher total pore numbers (+121.7 % TPN, p=0.005 and +83.3 % TPN, $p=0.033$, respectively) as well as higher average pore sizes (+39.0 % APA, $p = 0.007$ and +18.3 % APA $p = 0.044$, respectively) compared to DM patients.

When looking at the distribution of pores within the cortex at the distal radius, we observed —consistent with the results at the tibia—that the greatest differences in TPA, TPN, and APA between DMFx and DM subjects occurred at the midcortical layer, followed by the periosteal layer (Table 3). Interestingly, the results were even more pronounced at the distal radius than at the distal tibia. While at the distal tibia we observed a ~3-fold higher porosity (TPA) in the midcortical layer in DMFx vs DM subjects and a ~2-fold higher TPA in the periosteal layer in DMFx vs DM subjects, at the distal radius, we detected a ~14-fold higher TPA in the midcortical layer and a ~7-fold higher TPA in the periosteal layer in the DMFx group (see Table 3; +1327 % midcortical TPA in DMFx vs DM in distal radius, $p<0.001$; + 634 % periosteal TPA in DMFx vs DM in distal radius, $p=0.002$). We also noticed that the relative difference in cortical porosity by layer seemed to be factored upwards by three to five times in the distal radius, but in consistent percentage relative to the tibia. This resulted

in *p* values for almost all comparisons between DMFx and DM groups at the distal radius that were even more significant than at the distal tibia. Comparison of laminar metrics among the non-diabetic groups (Co vs Fx) and among the non-fractured groups (Co vs DM) did not yield any significant differences at either of the two skeletal sites.

Spatial pore distribution within each group

For each skeletal site, spatial pore distributions within each group are visualized in Fig. 1.

With respect to the distal tibial cortex, in all four groups, TPA, TPN, and APAwere high in the endosteal layer, lower in the midcortical subregion, and lowest in the periosteal subregion, generating a transcortical gradient of decreasing porosity, pore number, and size from the endosteum to the periosteum. Within this transcortical tibial gradient, differences between endosteal and periosteal values of porosity, pore number, and size were statistically significant within each group, with the exception of APA in the controls that showed a trend toward significance between endosteal and periosteal layers (endo APA vs peri APA, p=0.063). TPA values were 2.5 to 5.6-fold higher in the endosteal tibial layer compared to the periosteal tibial layer across all four groups. TPN values were 2.3 to 4.3-fold higher in the endosteal tibial layer compared to the periosteal tibial layer across all four groups.

When looking at the spatial pore distribution for the distal radius within each group we found, consistent with our tibia results, that the porosity formed a transcortical gradient with the highest TPA, TPN, and APA values in the endosteal layer and the lowest values in the periosteal layer. Moreover, we again observed a proportional scaling factor of the layer-wise porosity of the radius relative to the tibia. While at the tibia TPN was about 2.3 to 4.3 times higher in the endosteal vs periosteal layer across groups, at the radius, TPN was about 4.5 to 9.4 times higher in the endosteal compared to the periosteal layer (p<0.001).

Discussion

In this study, we aimed to investigate the spatial distribution of cortical pores at the tibia and radius in type 2 diabetic postmenopausal women with prior history of fragility fractures (DMFx, assigned high-risk group) and a fracture-free T2D group (DM, assigned low-risk group) and to compare their results to non-diabetic controls with (Fx) and without fragility fractures (Co) in order to better understand potential biological drivers and mechanical influences of T2D on cortical bone.

Our most striking finding was that at both skeletal sites, cortical porosity showed a different spatial distribution throughout the cortex depending on whether we examined the cortex of high-risk (DMFx) or low-risk T2D women (DM group). Compared to the low-risk T2D group, the high-risk fracture T2D group demonstrated an up to 14-fold increase in cortical porosity that was concentrated in the midcortical layer, followed by a moderate increase in porosity in the periosteal layer. Interestingly, the endosteal cortical layers-although showing the highest absolute levels of porosity across all groups-exhibited comparable amounts of cortical porosity in both diabetic groups in the tibia. From a bone biomechanical perspective, our results are in line with the observation of Burr et al. who stressed the impact of pore distribution for bone strength: pores located closer to the marrow cavity had a less

detrimental effect on bone mechanical properties than those located near the periosteal surface [14]. Given that cortical fractures have shown to start at microcracks located near increased cortical porosity [32] and that bending stresses are at maximum at the periosteal surfaces [33], the high preferential midcortical and periosteal distribution of pores in our high-risk T2D group could explain the higher skeletal fragility that was prevalent in this diabetic group.

Although the relative difference in cortical porosity was highest in the midcortical and periosteal layer between DMFx and DM groups, we also observed within each cohort and for both skeletal sites a transcortical porosity gradient, with the greatest porosity being exhibited in the endosteal layer. Such a gradient of cortical porosity is in good agreement with the existing literature [14] and is commonly for the most part explained as a result of bone aging and the so-called age-related cortical drift [34]: while young individuals' cortical porosity tends to be homogenously distributed throughout the cortex, aging (beyond the age of 40 years) leads to bone resorption mainly along the endocortical surface resulting in increased endocortical porosity [14]. At the same time, some bone is compensatorily deposited at the periosteal boundary, constitutively resulting in a relative low periosteal porosity (compared to endosteal layer) and leading to an increase in bone diameter. The transcortial gradient that we observed in all of our subjects (who all were postmenopausal women of at least 55 years or older) might therefore represent the bone microarchitectural snapshot-equivalent of these changes. If and how this increased endosteal porosity also contributes to fracture initiation is to date not clear. The fact that endosteal porosity was consistently greatest across all groups, even in the healthy control group makes an involvement in fracture initiation less likely. However, from a microstructural point of view, studies have shown that an increase in osteonal density goes along with a decline in fracture toughness, namely a decline in microcrack initation toughness and microcrack growth toughness [35, 36]. In addition, recent experimental evidence suggests that cortical fractures initiate particularly at microcracks that are located near elevated cortical porosity [32]. The higher number and size of cortical pores that we observed in the endosteal layer may therefore facilitate fracture initiation. However, future studies are needed to investigate and validate these hypotheses in vivo.

When comparing our results to the current literature, we found that different conditions affecting bone metabolism were linked to different spatial cortical pore distribution patterns. In a longitudinal study of osteopenic women, we observed that cortical porosity increased exclusively in the endosteal layer [37]. In another study examining the effect of disuse on bone, we found a longitudinal increase in cortical porosity uniformly throughout the cortex [38]. In contrast, the results of a recent cross-sectional study by Nirody et al. using the same layer analysis technique indicated that age-related increases in porosity are most extreme in the midcortical layer [17].

In synopsis, these data give cause to hypothesize that the different patterns of pore distribution that we observed in different diseases may be reflective of unique underlying biological mechanisms.

Although our study was focused on T2D, it is interesting that we also observed—similar to Nirody et al. [17]—the highest increase in cortical porosity in the midcortical layer in our high-risk T2D group when compared to the low-risk T2D group. From a clinical perspective, our high-risk DMFx subjects were slightly but not significantly older than the low-risk DM participants. Both groups showed similar poor glycemic control with an HbA1c in the range of 7.9 %. However, DMFx subjects had been suffering from T2D for a significantly longer time than DM individuals, making these DMFx individuals exposed for an average of 13 years to the detrimental effects of prolonged diabetic hyperglycemia [18]. As T2D is considered to cause accelerated body aging [39], this increased midcortical porosity in DMFx patients may be in part attributable to an accelerated bone aging, a phenomenon that we have already observed in this specific cohort at other skeletal sites such as proximal femur [20] and the radius [18].

Unlike Nirody et al. [17], we observed in addition to the pronounced increase in midcortical porosity also a less pronounced but still moderate increase in periosteal porosity at both skeletal sites in the DMFx group. The mechanisms underlying this increased porosity in the outer two thirds of the cortex of these patients are to date not known. Potential explanations could involve T2D-induced changes in bone's response to loading [40] or changes in cortical vascularization. In addition, studies have shown that a longer T2D duration is associated with an increased accumulation of advanced glycosylation endproducts (AGEs) which scale with higher rates of osteoblast apoptosis [41] and a higher osteoclast resorptive activity [42]. Moreover, a longer T2D duration was also found associated with a higher amount of microvascular and macrovascular diabetic complications [43]. In this context, it is remarkable that a recent HR-pQCTstudy established for the first time a link between higher overall cortical porosity and the presence of microvascular complications in T2D individuals [44]. In this light and given that midcortical and periosteal layers are highly susceptible, so-called watershed zones of the bony cortex [45, 46], one might speculate that the increased midcortical and periosteal porosity that we observed in the DMFx group may be driven by T2D-induced alterations in cortical vascularization. However, further histological and functional studies of the intraosseous vessels in diabetic bone are needed to elucidate the vascular effects of diabetic microangiopathy on (cortical) bone.

Although diabetes has been associated with alterations in the bone marrow [47] and bone marrow fat composition [48], we did not observe a change in endosteal porosity in any of the diabetic or non-diabetic groups at the distal tibia. For the radius, endosteal porosity was slightly higher in the DMFx group compared to DM subjects, but these relative differences were still subtle compared to the large differences in midcortical and periosteal porosity that we noted in this specific patient group. This makes it less likely that the significantly higher cortical porosity that we observed in DMFx subjects may be driven by mechanisms such as bone marrow expansion through trabecularization of the cortex, as such an expansion would affect the endosteal layer first.

With respect to the assignment of pores to the layers, it seems at the first glance somewhat concerning that some of the DMFx patients showed very large pores [18] that could introduce a "central tendency" bias resulting in the predominant assignment of pores to the midcortical layer. However, when we reviewed in detail the original HR-pQCT images of all

the DMFx subjects, we found that the majority of DMFx subjects showed increased but fine, well-dispersed and circumscribed pores, very similar to the mean porosity that is depicted in Fig. 2. Even when looking at the DMFx subject with the most extreme pore size, we saw only a few pores extending more than one pixel into the neighboring layer. When we additionally reran the statistical analysis excluding those DMFx cases showing the largest pores, our HR-pQCT results did not change (data not shown). The midcortical layer and the periosteal layer still showed the highest significant increases in porosity in DMFx groups compared to DM subjects. Taken together, we therefore believe that our results can be interpreted with confidence in the pore assignment technique and that our results are not driven by those “extreme” DMFx cases with the largest pore sizes.

Our study has several limitations. First, this cross-sectional study was mainly exploratory in nature and the number of subjects enrolled was therefore relatively limited (n = 20 per group). However, a priori power analyses for both skeletal sites (distal tibia and radius) revealed that despite this relatively small sample size, our study was sufficiently powered (power of 99.9 % at distal tibia and power of 90 % at distal radius) to detect differences in laminar cortical pore volume between the diabetic groups, at levels of significance ranging from p = 0.01 to p=0.001. The sufficient power of our study size is also reflected in the fact that we did observe statistical significant differences in cortical laminar metrics at both skeletal sites (see Tables 2 and 3). Although our study was sufficiently powered, future studies are desirable to validate our findings in a larger cohort. Limb dominance has recently been found to impact bone microarchitecture, and a lower cortical porosity was reported for the dominant relative to the non-dominant tibia [49]. Reviewing limb dominance in all of our patients, we observed that 97.3 % of all radius scans (and 100 % of all DMFx and DM radius scans) were acquired at the non-dominant radius. For the tibia, only 2 out of 20 patients in the DMFx groups had been scanned at the dominant tibia due to residual surgical metal at the non-dominant side which had never been removed. These findings make it unlikely that limb dominance might have influenced our results. With respect to the tibia, these findings suggest further that the magnitude of our tibial cortical porosity differences between DMFx and DM subjects would have been even more pronounced if these two DMFx patients had been scanned at the non-dominant tibia. Another pertinent limitation is that we analyzed the tibia and radius cortex via HR-pQCT, which imposes limitations with respect to image resolution. Cortical bone is organized in hierarchical levels, starting from the lamella to the first-level structures such as Haversian canals and resorption cavities (80 to 500 μm) down to lacunae and canaliculi as second-level (5 to 20 μm) structures [50, 51]. Despite providing the highest resolution that is currently possible for in vivo bone imaging, HR-pQCT is only able to resolve pores that are larger than approximately 100 μm in diameter [17]. That is, HR-pQCT can resolve larger Haversian canals and resorptive cavities but cannot resolve micropores that might represent osteocyte lacunae or canaliculi, unless they had enlarged to a detectable (>100 μm) size. Given that DM and DMFx differed mainly in their diabetic duration, it is possible that T2D affects the bone first on a microporous level, leading to micropores that are not detectable with HR-pQCT. Disease progression might then shift the pores into a resolvable size. Further high-resolution studies are needed to longitudinally assess T2D bone-and porosity changes below 100 μm and assess if this hypothesis is true. However, as evidence shows that larger pores have a more dramatic effect

on mechanical properties [36], we believe that HR-pQCT resolves the relevant porosity that is associated with the higher fragility risk in DMFx. The method by which pores are assigned to a cortical layer in the laminar analysis technique presents another potential limitation. Each pore is “skeletonized” or reduced to its centroid prior to being assigned to a single layer. Therefore, the laminar analysis technique does not account for pores that cross borders between layers but rather assigns the entire pore area to the single layer in which the centroid resides. This limits our ability to interpret the distribution of partial pores among layers. Finally, the software algorithm and the layer separation depend heavily on the proper segmentation of the cortical boundaries. These might be difficult to define in particular in cases with increased trabecularization of the cortex [16]. To assure most appropriate segmentation of the cortical boundaries, all boundaries were checked by an experienced radiologist (JMP) who confirmed that even in the DMFx group, the endocortical boundaries were still visually distinguishable.

In summary, our findings of increased midcortical and periosteal porosity in DMFx patients suggest that unique mechanisms—such as diabetes-related vascular changes—may be acting within these two layers in type 2 diabetic women with history of fragility fractures. Longitudinal studies are needed to investigate whether cortical porosity is the anatomic counterpart of T2D-induced vascular cortical changes. In addition, cortical pore laminar analysis is a helpful tool in defining and distinguishing metabolic bone conditions such as diabetic bone disease from other bone affecting conditions such as osteopenia and disuse on a microstructural level. Future studies should apply this technique longitudinally and to other cohorts with pathological cortical porosity, such as patients suffering from hyperparathyroidism.

Acknowledgments

This study was supported by the National Institutes of Health grants NIH R01-AG17762, R03-AR064004, and K01 AR 056734 to GK, RC1 AR058405 to TML, and R01 AR060700 to AJB and the Erwin Schrödinger grant (J-3079 to JMP), the QUEST Scholarship program to KC, and The University of Berkeley Undergraduate Research Apprentice Program (URAP Berkeley) to JN. We thank Thelma Munoz and Melissa Guan for their help in recruiting and in consenting the patients.

Compliance with ethical standards

Conflicts of interest Dr. Burghardt serves as consultant for Ultragenyx Pharmaceutical Inc., and Dr. Link received grant money from NIH-NIAMS. Dr. Heilmeier received travel funds from ASBMR. Karen Cheng, Robin Parrish, Jasmine Nirody, Janina M. Patsch, Chiyuan A. Zhang, Gabby B. Joseph, Ann V. Schwartz, and Galateia Kazakia declare that they have no conflict of interest.

References

1. Ruppel ME, Miller LM, Burr DB (2008) The effect of the microscopic and nanoscale structure on bone fragility. Osteoporos Int 19: 1251–1265 [PubMed: 18317862]
2. Augat P, Schorlemmer S (2006) The role of cortical bone and its microstructure in bone strength. Age Ageing 35(Suppl 2):ii27–ii31 3. Currey JD (1988) The effect of porosity and mineral content on the [PubMed: 16926200]
3. Currey JD (1988) The effect of porosity and mineral content on the Young’s modulus of elasticity of compact bone. J Biomech 21:131–139 [PubMed: 3350827]
4. Schaffler MB, Burr DB (1988) Stiffness of compact bone: effects of porosity and density. J Biomech 21:13–16 [PubMed: 3339022]

5. Ural A, Vashishth D (2007) Effects of intracortical porosity on fracture toughness in aging human bone: a microCT-based cohesive finite element study. J Biomech Eng 129:625–631 [PubMed: 17887887]
6. McCalden RW, McGeough JA, Barker MB, Court-Brown CM (1993) Age-related changes in the tensile properties of cortical bone. The relative importance of changes in porosity, mineralization, and microstructure. J Bone Joint Surg 75:1193–1205 [PubMed: 8354678]
7. Yeni YN, Brown CU, Wang Z, Norman TL (1997) The influence of bone morphology on fracture toughness of the human femur and tibia. Bone 21:453–459 [PubMed: 9356740]
8. Bala Y, Zebaze R, Ghasem-Zadeh A et al. (2014) Cortical porosity identifies women with osteopenia at increased risk for forearm fractures. J Bone Miner Res 29:1356–1362 [PubMed: 24519558]
9. Burghardt AJ, Kazakia GJ, Sode M, de Papp AE, Link TM, Majumdar S (2010) A longitudinal HR-pQCTstudy of alendronate treatment in postmenopausal women with low bone density: relations among density, cortical and trabecular microarchitecture, biomechanics, and bone turnover. J Bone Miner Res 25:2558–2571 [PubMed: 20564242]
10. Bala Y, Chapurlat R, Cheung AM et al. (2014) Risedronate slows or partly reverses cortical and trabecular microarchitectural deterioration in postmenopausal women. J Bone Miner Res 29:380–388 [PubMed: 24115129]
11. Borah B, Dufresne T, Nurre J, Phipps R, Chmielewski P, Wagner L, Lundy M, Bouxsein M, Zebaze R, Seeman E (2010) Risedronate reduces intracortical porosity in women with osteoporosis. J Bone Miner Res 25:41–47 [PubMed: 19580469]
12. Atkinson PJ (1965) Changes in resorption spaces in femoral cortical bone with age. J Pathol Bacteriol 89:173–178 [PubMed: 14263459]
13. Squillante RG, Williams JL (1993) Video densito metry of osteons in females with femoral neck fractures. Calcif Tissue Int 52:273–277 [PubMed: 8467407]
14. Burr DB (2010) Cortical bone: a target for fracture prevention? Lancet 375:1672–1673 [PubMed: 20472154]
15. Jordan GR, Loveridge N, Bell KL, Power J, Rushton N, Reeve J (2000) Spatial clustering of remodeling osteons in the femoral neck cortex: a cause of weakness in hip fracture? Bone 26:305–313 [PubMed: 10710006]
16. Zebaze RM, Ghasem-Zadeh A, Bohte A, Iuliano-Burns S, Mirams M, Price RI, Mackie EJ, Seeman E (2010) Intracortical remodelling and porosity in the distal radius and post-mortem femurs of women: a cross-sectional study. Lancet 375:1729–1736 [PubMed: 20472174]
17. Nirody JA, Cheng KP, Parrish RM, Burghardt AJ, Majumdar S, Link TM, Kazakia GJ (2015) Spatial distribution of intracortical porosity varies across age and sex. Bone 75:88–95 [PubMed: 25701139]
18. Patsch JM, Burghardt AJ, Yap SP, Baum T, Schwartz AV, Joseph GB, Link TM (2013) Increased cortical porosity in type 2 diabetic postmenopausal women with fragility fractures. J Bone Miner Res 28:313–324 [PubMed: 22991256]
19. Samelson E, Bouxsein M, Brochin E et al. (2014) Deficits in cortical bone density and microstructure in type 2 diabetes: framingham HR-pQCT study. J Bone Miner Res 29:S28–S28
20. Heilmeier U, Carpenter DR, Patsch JM, Harnish R, Joseph GB, Burghardt AJ, Baum T, Schwartz AV, Lang TF, Link TM (2015) Volumetric femoral BMD, bone geometry, and serum sclerostin levels differ between type 2 diabetic postmenopausal women with and without fragility fractures. Osteoporos Int 26:1283–1293 [PubMed: 25582311]
21. American Diabetes Association (2012) Standards of medical care in diabetes—2012. Diabetes Care 35(Suppl 1):S11–S63 [PubMed: 22187469]
22. Levey AS, Coresh J, Balk E, Kausz AT, Levin A, Steffes MW, Hogg RJ, Perrone RD, Lau J, Eknoyan G (2003) National Kidney Foundation practice guidelines for chronic kidney disease: evaluation, classification, and stratification. Ann Intern Med 139:137–147 [PubMed: 12859163]
23. Miller WG (2009) Estimating glomerular filtration rate. Clin Chem Lab Med 47:1017–1019 [PubMed: 19728841]
24. Link T, Heilmeier U (2016) Bone quality—beyond BMD. Semin Musculoskelet Radiol

25. Nishiyama KK, Shane E (2013) Clinical imaging of bone microarchitecture with HR-pQCT. Curr Osteoporos Rep 11:147–155 [PubMed: 23504496]
26. Boutroy S, Bouxsein ML, Munoz F, Delmas PD (2005) In vivo assessment of trabecular bone microarchitecture by high-resolution peripheral quantitative computed tomography. J Clin Endocrinol Metab 90:6508–6515 [PubMed: 16189253]
27. Khosla S, Riggs BL, Atkinson EJ, Oberg AL, McDaniel LJ, Holets M, Peterson JM, Melton LJ 3rd (2006) Effects of sex and age on bone microstructure at the ultradistal radius: a population-based noninvasive in vivo assessment. J Bone Miner Res 21:124–131 [PubMed: 16355281]
28. Pialat JB, Burghardt AJ, Sode M, Link TM, Majumdar S (2012) Visual grading of motion induced image degradation in high resolution peripheral computed tomography: impact of image quality on measures of bone density and micro-architecture. Bone 50:111–118 [PubMed: 22019605]
29. Burghardt AJ, Buie HR, Laib A, Majumdar S, Boyd SK (2010) Reproducibility of direct quantitative measures of cortical bone microarchitecture of the distal radius and tibia by HR-pQCT. Bone 47:519–528 [PubMed: 20561906]
30. Tjong W, Kazakia GJ, Burghardt AJ, Majumdar S (2012) The effect of voxel size on high-resolution peripheral computed tomography measurements of trabecular and cortical bone microstructure. Med Phys 39:1893–1903 [PubMed: 22482611]
31. Tjong W, Nirody J, Burghardt AJ, Carballido-Gamio J, Kazakia GJ (2014) Structural analysis of cortical porosity applied to HR-pQCT data. Med Phys 41:013701 [PubMed: 24387533]
32. Turnbull TL, Baumann AP, Roeder RK (2014) Fatigue microcracks that initiate fracture are located near elevated intracortical porosity but not elevated mineralization. J Biomech 47:3135–3142 [PubMed: 25065731]
33. Whiting WC, Zernicke RF (2008) Biomechanics of musculoskeletal injury. Human Kinetics, Champaign, Ill.
34. Boskey AL, Coleman R (2010) Aging and bone. J Dent Res 89: 1333–1348 [PubMed: 20924069]
35. Nalla RK, Kruzic JJ, Kinney JH, Balooch M, Ager JW III, Ritchie RO (2006) Role of microstructure in the aging-related deterioration of the toughness of human cortical bone. Mater Sci Eng C 26:1251–1260
36. Zimmermann EA, Schaible E, Bale H, Barth HD, Tang SY, Reichert P, Busse B, Alliston T, Ager JW 3rd, Ritchie RO (2011) Age-related changes in the plasticity and toughness of human cortical bone at multiple length scales. Proc Natl Acad Sci U S A 108: 14416–14421 [PubMed: 21873221]
37. Tjong W, Nirody J, Carballido-Gamio J, B A, Patsch J, Majumdar S, Kazakia G (2012) Longitudinal analysis of cortical pore structure using HR-pQCT. J Bone Miner Res 27.
38. Kazakia GJ, Tjong W, Nirody JA, Burghardt AJ, Carballido-Gamio J, Patsch JM, Link T, Feeley BT, Ma CB (2014) The influence of disuse on bone microstructure and mechanics assessed by HR-pQCT. Bone 63:132–140 [PubMed: 24603002]
39. Frassetto LA, Sebastian A (2012) How metabolic acidosis and oxidative stress alone and interacting may increase the risk of fracture in diabetic subjects. Med Hypotheses 79:189–192 [PubMed: 22583559]
40. Parajuli A, Liu C, Li W, Gu X, Lai X, Pei S, Price C, You L, Lu L, Wang L (2015) Bone's responses to mechanical loading are impaired in type 1 diabetes. Bone 81:152–160, Abstracts [PubMed: 26183251]
41. Alikhani M, Alikhani Z, Boyd C, MacLellan CM, Raptis M, Liu R, Pischon N, Trackman PC, Gerstenfeld L, Graves DT (2007) Advanced glycation end products stimulate osteoblast apoptosis via the MAP kinase and cytosolic apoptotic pathways. Bone 40: 345–353 [PubMed: 17064973]
42. Dong XN, Qin A, Xu J, Wang X (2011) In situ accumulation of advanced glycation endproducts (AGEs) in bone matrix and its correlation with osteoclastic bone resorption. Bone 49:174–183 [PubMed: 21530698]
43. Brownlee M (2005) The pathobiology of diabetic complications: a unifying mechanism. Diabetes 54:1615–1625 [PubMed: 15919781]
44. Shanbhogue VV, Hansen S, Frost M, Jorgensen NR, Hermann AP, Henriksen JE, Brixen K (2015) Compromised cortical bone compartment in type 2 diabetes mellitus patients with microvascular disease. Eur J Endocrinol 174:115–124 [PubMed: 26537860]

45. Trueta J (1974) Blood supply and the rate of healing of tibial fractures. Clin Orthopaed Rel Res 11–26

46. Bogousslavsky J, Moulin T (1995) Borderzone Infarcts In: Bogousslavsky J (ed) Stroke Syndromes. Cambridge University Press, Cambridge, pp 358–365

47. Bhansali A, Asokumar P, Walia R, Bhansali S, Gupta V, Jain A, Sachdeva N, Sharma RR, Marwaha N, Khandelwal N (2014) Efficacy and safety of autologous bone marrow-derived stem cell transplantation in patients with type 2 diabetes mellitus: a randomized placebo-controlled study. Cell Transplant 23:1075–1085 [PubMed: 23561959]

48. Patsch JM, Li X, Baum T, Yap SP, Karampinos DC, Schwartz AV, Link TM (2013) Bone marrow fat composition as a novel imaging biomarker in postmenopausal women with prevalent fragility fractures. J Bone Miner Res 28:1721–1728 [PubMed: 23558967]

49. Hildebrandt EM, Manske SL, Hanley DA, Boyd SK (2015) Bilateral asymmetry of radius and tibia bone macroarchitecture and microarchitecture: a high-resolution peripheral quantitative computed tomography study. J Clin Densitom

50. Bousson V, Meunier A, Bergot C, Vicaut E, Rocha MA, Morais MH, Laval-Jeantet AM, Laredo JD (2001) Distribution of intracortical porosity in human midfemoral cortex by age and gender. J Bone Miner Res 16:1308–1317 [PubMed: 11450707]

51. Cooper DM, Thomas CD, Clement JG, Turinsky AL, Sensen CW, Hallgrimsson B (2007) Age-dependent change in the 3D structure of cortical porosity at the human femoral midshaft. Bone 40:957–965 [PubMed: 17223618]

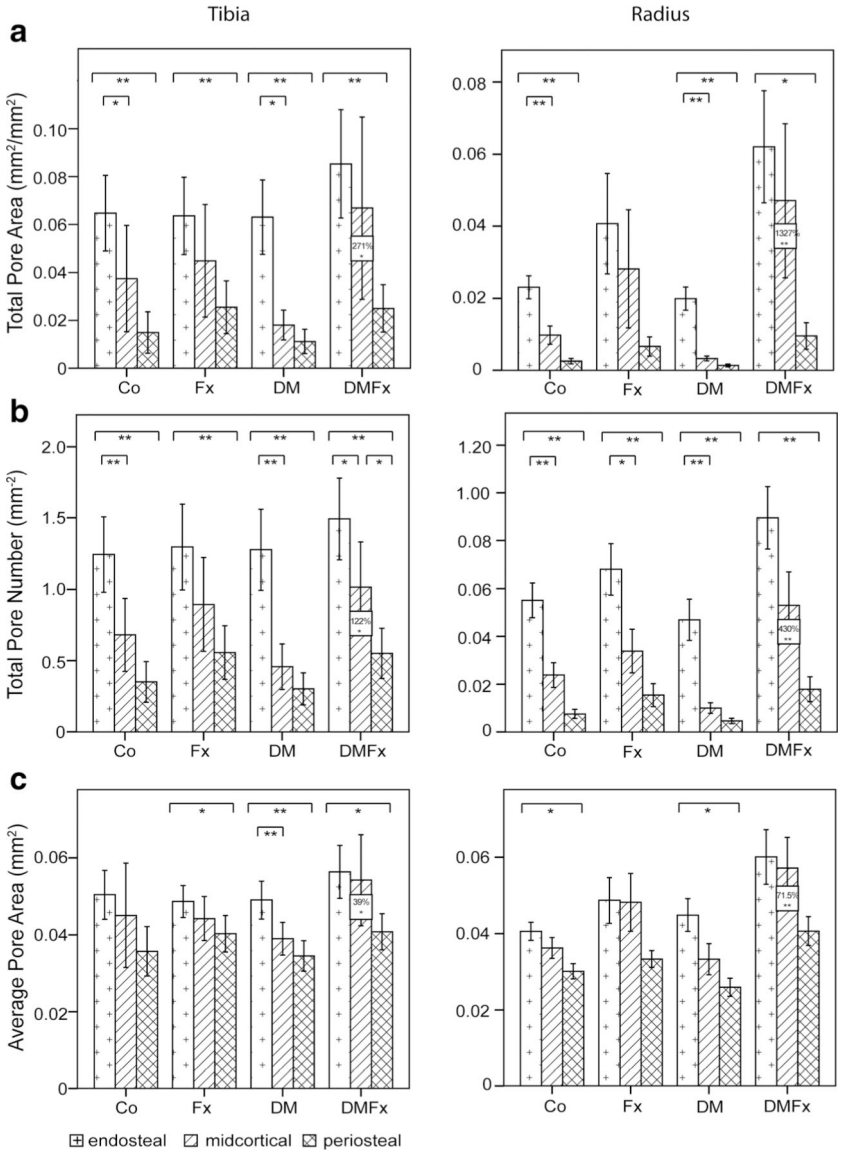

Fig. 1.

Results of laminar cortical analysis by cortical layer, group, and by skeletal site. Results for the distal tibia are displayed on the *left*; results for the distal radius are shown on the *right*. *Co* controls, *Fx* women with history of fragility fractures, *DM* type 2 diabetic (T2D) women without fractures, *DMFx* T2D women with history of fragility fractures. *Bars* indicate differences between layers; *boxed values* indicate significant differences between DMFx and DM groups. $^{**}p \leq 0.001$, $^{*}p \leq 0.05$

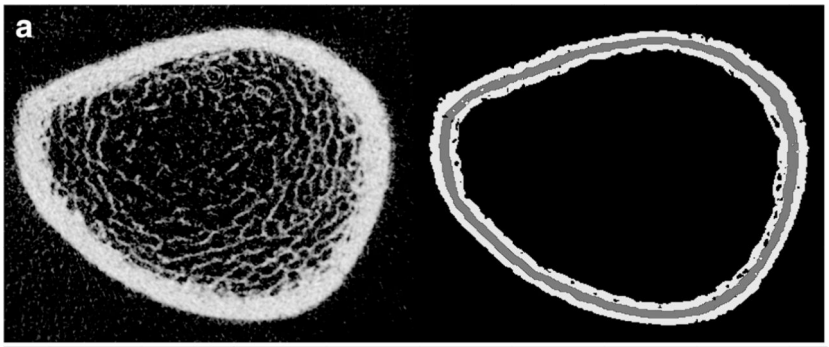

Exact Metrics	Total Pore Area (mm^2/ mm^2)			Total Pore Number (/mm^2)			Average Pore Area (mm^2)		
Participant	End	Mid	Peri	End	Mid	Peri	End	Mid	Peri
DM subject	0.0697	0.0126	0.0101	1.33	0.42	0.33	0.052	0.030	0.0304
Overall DM group	0.0630	0.0180	0.0112	1.28	0.46	0.30	0.049	0.039	0.0345

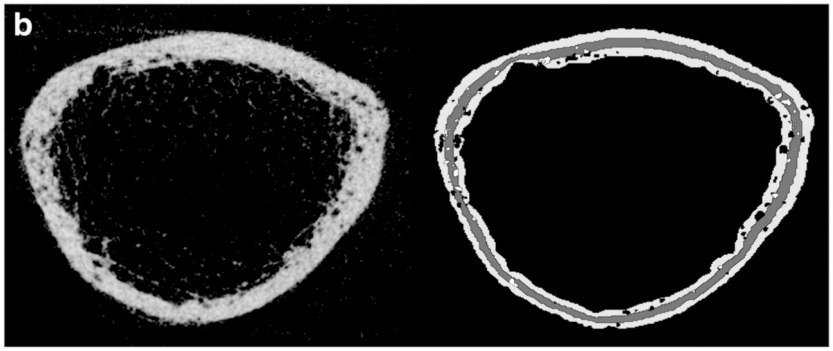

Exact Metrics	Total Pore Area (mm^2/ mm^2)			Total Pore Number (/mm^2)			Average Pore Area (mm^2)		
Participant	End	Mid	Peri	End	Mid	Peri	End	Mid	Peri
DMFx subject	0.0693	0.0529	0.0153	1.37	1.12	0.40	0.051	0.047	0.039
Overall DMFx group	0.0853	0.0668	0.0250	1.49	1.02	0.55	0.056	0.054	0.041

Fig. 2.

Two representative HR-pQCT axial cross sections from the distal tibia scans of **a)** a type 2 diabetic postmenopausal woman without history of fragility fractures (DM) and of **b)** a type 2 diabetic postmenopausal woman with history of fragility fractures (DMFx). HR-pQCT cross sections (on the *left*) are displayed alongside the cortical pore laminar mask delineating the pores within the three cortical layers (on the *right*). The table below summarizes the exact TPA, TPN, and APA values per layer for the given subject and displays for comparison the mean TPA, TPN, and APA values of the overall diabetic group the subject belongs to. Pores classified as endosteal and periosteal are delineated in *black*; pores classified as midcortical are visualized in *white*

Table 1

Descriptive characteristics of all study participants with HR-pQCT measurements and cortical laminar analysis (*n*=79)

	Co (*n*=20)	Fx (*n*=20)	DM (*n*=19)	DMFx (*n*=20)	*p* values DMFx vs DM
Demographics and anthropometry					
Age (years)	58.0±4.8	64.5±5.7[a]	59.5±4.1	63.3±6.0[a]	*p*=0.117
Body mass index (kg/m^2)	26.0±4.7	25.3±3.4	27.7±3.8	28.9±5.5	*p*=0.838
Racial composition					
Caucasian (%)	60.0 %	85.0 %	36.8 %	40.0 %	*p*=0.667
Asian (%)	25.0 %	10.0 %	36.8 %	25.0 %	
African-American (%)	5.0 %	0.0 %	15.8 %	30.0 %	
Hispanic (%)	10.0 %	5.0 %	5.3 %	0.0 %	
Pacific Islander/Native Hawaiian (%)	0.0 %	0.0 %	5.3 %	5.0 %	
Diabetic and metabolic status					
Duration of type 2 diabetes (years)	n.a.	n.a.	7.6±3.1	13.3±8.8	***p*=0.012**
HbA1c (%)	5.8±0.3	5.9±0.4	7.8±1.6	7.9±2.7	*p*=0.999
Fasting glucose (mg/dL)	91.8±11.9	91.5±11.6	162.9±70.6	148.7±68.9	*p*=0.809
PTH (pg/mL)	37.3±14.0	33.5±23.8	38.2±16.1	41.4±25.5	*p*=0.962
25-OH vitamin D (ng/mL)	28.6±11.4	42.1±11.4[a]	26.6±11.3	32.7±12.6	*p*=0.375
Estimated glomerular filtration (eGFR)	87.8	83.5	98.6	89.3	*p*=0.465
Rate (mL/min/1.73 m^2)	[77.3–98.0]	[69.0–86.3]	[79.0–117.9]	[69.2–101.7]	
Fracture status and history					
Time since last fragility fracture (years)		3.3±3.6		3.1±2.7	*p*=0.835
Prevalence of fragility fractures (n)		23		32	*p*=0.333
Time since last fragility fracture	n.a.	≥5 months	n.a.	≥5 months	
MR spine – occult acute vertebral fx (%)	0 %	0 %	0 %	0 %	

Intergroup differences were assessed using analysis of variance (ANOVA) with subsequent post hoc Tukey tests or independent *t* tests or Pearson's chisquared test as appropriate. Non-diabetic postmenopausal women without history of fragility fractures (*Co*), non-diabetic postmenopausal women with history of fragility fractures (*Fx*), type 2 diabetic (T2D) postmenopausal women without any history of fragility fracture (*DM*), and T2D postmenopausal women with a positive history of fragility fractures after the onset of diabetes (*DMFx*). Data are expressed as unadjusted means±SD. eGFR is expressed as median [25th–75th percentile]. Significant *p* values ($p < 0.05$) are marked in bold print. Presented *p* values were calculated using either independent *t*-test or Pearson's χ^2 test, as appropriate

n.a. not applicable

[a]Statistical significant difference vs Co group

Table 2

Laminar analysis metrics of the distal tibia displayed per group: non-diabetic postmenopausal women with (Fx) and without (Co) history of fragility fractures and T2D postmenopausal women with (DMFx) and without history of fragility fractures (DM) after the onset of T2D

Co (*n*=20)	Fx (*n*=20)	DM (*n*=19)	DMFx >(*n*=20)	Dm vs DMFx % relative difference	Dm vs DMFx *p* value
Total pore area (TPA) (mm^2/mm^2)					
Endosteal TPA 0.0647±0.03	0.0636±0.03	0.0630±0.03	0.0853±0.05	+35.4 %	*p*=0.169
Midcortical TPA 0.0374±0.05	0.0448±0.05	0.0180±0.01	0.0668±0.08	+271.1 %	***p*=0.001**
Periosteal TPA 0.0149±0.02	0.0255±0.02	0.0112±0.01	0.0250±0.02	+123.2 %	***p*=0.028**
Total pore number (TPN) (mm^{-2})					
Endosteal TPN 1.24±0.56	1.30±0.64	1.28±0.59	1.49±0.61	+16.4 %	*p*=0.216
Midcortical TPN 0.68±0.55	0.89±0.70	0.46±0.33	1.02±0.67	+121.7 %	***p*=0.005**
Periosteal TPN 0.35±0.31	0.56±0.40	0.30±0.23	0.55±0.38	+83.3 %	***p*=0.033**
Average pore area (APA) (mm^2)					
Endosteal APA 0.0504±0.01	0.0487±0.01	0.0490±0.01	0.0563±0.01	+14.9 %	*p*=0.136
Midcortical APA 0.0451±0.03	0.0442±0.01	0.0390±0.01	0.0542±0.03	+39.0 %	***p*=0.007**
Periosteal APA 0.0358±0.01	0.0403±0.01	0.0345±0.01	0.0408±0.01	+18.3 %	***p*=0.043**

Total pore area (TPA) (mm^2/mm^2), total pore number (TPN) (mm^{-2}), and average pore area (APA) (mm^2) were calculated for each layer. TPA and TPN were normalized by the area of each layer. All values are reported as the average across all slices. Data are expressed as unadjusted means±SD.

Significant *p* values are highlighted in bold

Table 3

Laminar analysis metrics of the distal radius displayed per group: non-diabetic postmenopausal women with (Fx) and without (Co) history of fragility fractures and T2D postmenopausal women with (DMFx) and without history of fragility fractures (DM) after the onset of T2D

Co (*n*=19)	Fx (*n*=20)	DM (*n*=17)	DMFx (*n*=18)	Dm vs DMFx % relative difference	Dm vs DMFx *p* value
Total pore area (TPA) (mm^2/mm^2)					
Endosteal TPA 0.0231±0.01	0.0407±0.06	0.0199±0.01	0.0621±0.07	+212 %	*p*=0.004
Midcortical TPA 0.0098±0.01	0.0282±0.07	0.0033±0.01	0.0471±0.09	+1327 %	***p*=0.000**
Periosteal TPA 0.0025±0.01	0.0066±0.01	0.0013±0.01	0.0095±0.02	+634 %	***p*=0.002**
Total pore number (TPN) (mm^{-2})					
Endosteal TPN 0.55±0.32	0.68±0.48	0.47±0.36	0.89±0.55	+89.4 %	*p*=0.006
Midcortical TPN 0.24±0.23	0.34±0.41	0.10±0.09	0.53±0.59	+430 %	***p*=0.000**
Periosteal TPN 0.08±0.09	0.15±0.22	0.05±0.05	0.18±0.22	+289 %	***p*=0.006**
Average pore area (APA) (mm^2)					
Endosteal APA 0.0406±0.01	0.0487±0.03	0.0449±0.02	0.0601±0.03	+33.9 %	*p*=0.092
Midcortical APA 0.0362±0.01	0.0482±0.03	0.0333±0.02	0.0571±0.03	+71.5 %	***p*=0.000**
Periosteal APA 0.0301±0.01	0.0334±0.01	0.0259±0.01	0.0406±0.02	+56.8 %	***p*=0.002**

Total pore area (TPA) (mm^2/mm^2), total pore number (TPN) (mm^{-2}), and average pore area (APA) (mm^2) were calculated for each layer. TPA and TPN were normalized by the area of each layer. All values are reported as the average across all slices. Data are expressed as unadjusted means ± SD.

Significant *p* values are highlighted in bold